High-Power Laser Diodes with High Polarization Purity

Etai Rosenkrantz, Dan Yanson*, Ophir Peleg, Moshe Blonder, Noam Rappaport, and Genady Klumel.
SCD – SemiConductor Devices, P.O.Box 2250/99, Haifa 31021, Israel

ABSTRACT

Fiber coupled modules need power scaling for fiber laser pumping. To this end, techniques such as geometrical, spectral and polarization beam combining (PBC) are used. For PBC, linear polarization with high degree of purity is important, as any non-perfectly polarized light leads to losses and heating. Furthermore, PBC is typically performed in a collimated portion of the beams, which also cancels the angular dependence of the PBC element, e.g., beam-splitter. However, we discovered that laser diodes (LDs) have variable degrees of polarization, which depends both on the operating current and far-field divergence. We present data to show angle-resolved polarization measurements that correlate with the ignition of high-order modes in the slow-axis emission of the LD. We demonstrate that the ultimate laser brightness includes not only the standard parameters such as power, emitting area and beam divergence, but also the degree of polarization (DoP), which is a strong function of the latter. Improved slow-axis divergence, therefore, contributes not only to high brightness but also high beam combining efficiency through polarization.

Keywords: Degree of polarization, fiber coupling, laser diode, high-power laser, fiber coupled emitter, multi-emitter module, brightness, polarization beam combining, slow axis divergence.

1. INTRODUCTION

The demand for high-power, high-brightness fiber-coupled laser diodes is constantly on the rise, primarily due to solid-state and fiber laser pumping [1], [2]. Besides wattage, fiber laser makers require pump light to be delivered with high spatial (and spectral) brightness, typically using multi-emitter pumps pigtailed with an 0.15 - 0.22 numerical aperture (NA) fiber. A linear power scaling of diode lasers, especially single emitters, is limited by the degradation of efficiency and beam quality at high powers due to thermal effects [3]. Therefore, multi-emitter power scaling techniques are employed to multiplex several low-power beams using geometrical, spectral, and polarization beam combining (PBC).

PBC combines two linearly-polarized beams with the beam quality of a single input beam [3-7]. In PBC, the polarization purity, commonly characterized by Degree of Polarization (DoP), of each beam plays a crucial role in the combining efficiency, since a non-perfectly polarized beam will lead to losses due to parasitic light and heating [6]. The importance of both containing the slow axis emission within the fiber NA, and providing a high DoP for efficient PBC, is illustrated in Figure 1, which shows a typical single emitter geometrical and polarization multiplexing architecture. The polarization of the top emitter beam is rotated through 90° using a half-wave plate; it is then combined with the horizontal, unrotated polarization beam from a second emitter using a polarizing beam splitter (PBS) into an optical fiber. Note the parasitic light due to a DoP of <100%, which is lost in the process. PBC is typically performed in a collimated portion of the beams [5], which mitigates the angular sensitivity of the PBS.

While several DoP definitions exist in the literature, in this work we used one according to [8], where the fractions of TE and TM-polarized powers, P_{TE} and P_{TM} respectively, in a high-power laser beam add up to 100%:

$$DoP_{TE(TM)} = P_{TE(TM)}/(P_{TE} + P_{TM}) \quad (1)$$

In a strained InGaAs/AlGaAs material system typically employed in laser diodes at 9xx nm, optical transitions in a quantum well (QW) with the participation of heavy holes are only allowed for a single light polarization in which the electric field vector lies in the QW plane. Since light holes are prevented from radiative transitions by the built-in strain, the stimulated emission should ideally be 100% TE-polarized. However, the presence of heteroboundaries and symmetry breaking of atomic bonds at the boundaries associated with epitaxial growth, result in the mixing of states for heavy and

* dany@scd.co.il; phone +972 4 990 2711; fax + 972 4 990 2627; www.scd.co.il

light holes. Furthermore, a deviation of the QW potential from a rectangular profile can lower the linear DoP by 2–5%. A reduction in the degree of anisotropy enhances the contribution of light holes (TM polarization), with their energy levels approaching those of heavy holes [9], [10]. The TE DoP can be further reduced by external strain, e.g., high-stress surface metallization. Soldering diode lasers to a submount can also induce substantial mechanical strain. Strain fields typically accumulate at mechanical edges, such as the edge of trenches, metallization features (such as plating), or electrical contacts [11].

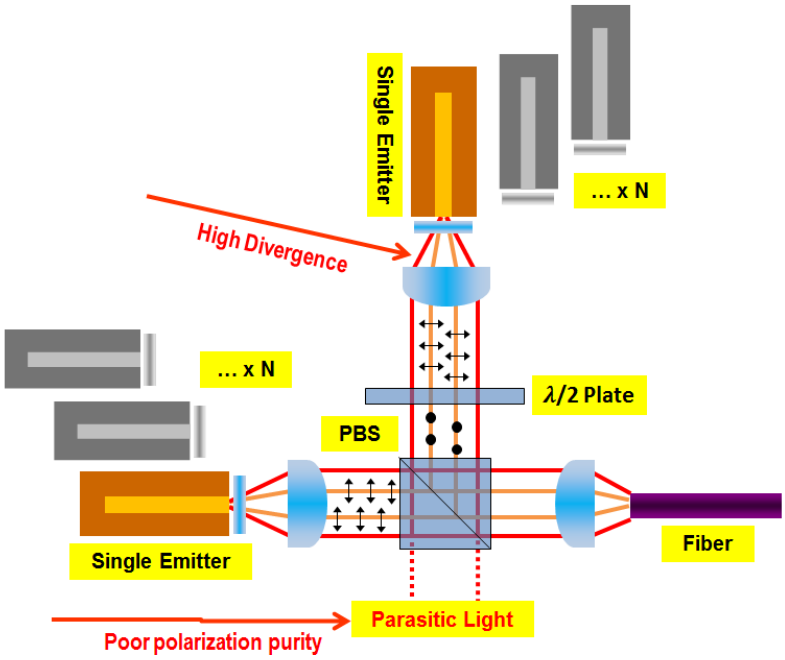

Figure 1. A typical fiber coupling architecture employing PBC of multiple single emitters.

Past studies have mostly focused on laser die packaging to maximize the polarization purity by relaxing the induced strain in a bonded laser chip [12], e.g., by employing thermal expansion-matched carriers and submounts for chip assembly, or a soft solder such as indium.

In this work, we demonstrate that high polarization purity can also be achieved by optimizing the wafer design of high-power single emitters, with the epitaxial waveguide itself providing additional selectivity for polarized lasing modes.

At SCD, we have set out to develop InGaAs/AlGaAs single emitter devices emitting at 975nm and offering both high spatial brightness (with a narrow slow-axis far-field) and high polarization purity (TE emission). We establish a clear correlation between these two characteristics, which prompts us to propose a definition for polarization brightness for PBC applications, as will be explained in Sec. 4.

The paper is organized as follows: we start off by describing our Al-based epitaxial design in Sec.2, which also includes the performance of the single emitters fabricated. In Sec. 3, we present the polarization methods and measurements of these emitters on our standard packaging platform. DoP simulation and brightness implications are discussed in Sec. 4, followed by conclusions in Sec.5.

2. EPITAXY & SINGLE EMITTERS

2.1 Epitaxial design

In order to achieve consistent device performance across several 9xx nm wavelengths, we have developed a common Al-based epitaxial platform utilizing an asymmetric structure design, with only minor changes to the InGaAs quantum well

thickness and position to allow for wavelength adjustment. By using an asymmetric waveguide structure, we reported a very low optical loss of under 0.5 cm^{-1} enabling wall-plug efficiencies in excess of 55% [13], [14].

The focus of our latest development campaign was to increase both the emitter brightness and polarization selectivity for the guided waveguide modes without compromising the laser efficiency. This has been achieved over two generations of epitaxial structures, Design A and B, by shifting and expanding the transverse optical mode away from absorbing p-doped layers.

Using the *FIMMWAVE* fully vectorial mode solvers by *Photon Design*, we performed a thorough design study of both transverse and lateral modes in a 95 µm-wide stripe waveguide with a view to enhancing guided lateral TE modes. The optimization involved the interplay among the vertical and lateral confinement, material composition, and waveguide asymmetry. Indeed, a similar parameter set is employed in [15] for exactly the opposite purpose, which is to achieve polarization *insensitivity* in semiconductor optical amplifiers. It is important to note that our simulation only concerned a "cold cavity" waveguide without any polarization selection afforded by the QW, or other effects such as carrier-induced refractive index change.

As a result, we have been able to increase the polarization sensitivity in favor of TE modes in our epitaxial Design B compared to baseline Design A. Figure 2(a) contains the simulated profiles of the first 11 lateral modes in Design A, with the first two having TM polarization followed by alternating TE/TM modes. By contrast, in optimized Design B, the 7 lowest modes of Figure 2(b) are TE, which provides for an extra selection rule towards a high DoP in addition to the TE-dominant QW gain.

At the same time, broad area laser emission is known to contain many more than 7 lateral modes [16]. It is also understood that TE modes will enjoy much higher QW gain than TM ones. But by minimizing the lateral mode content for higher spatial brightness in Design B, we should also be able to reduce the number of guided TM modes, thus improving its TE polarization purity.

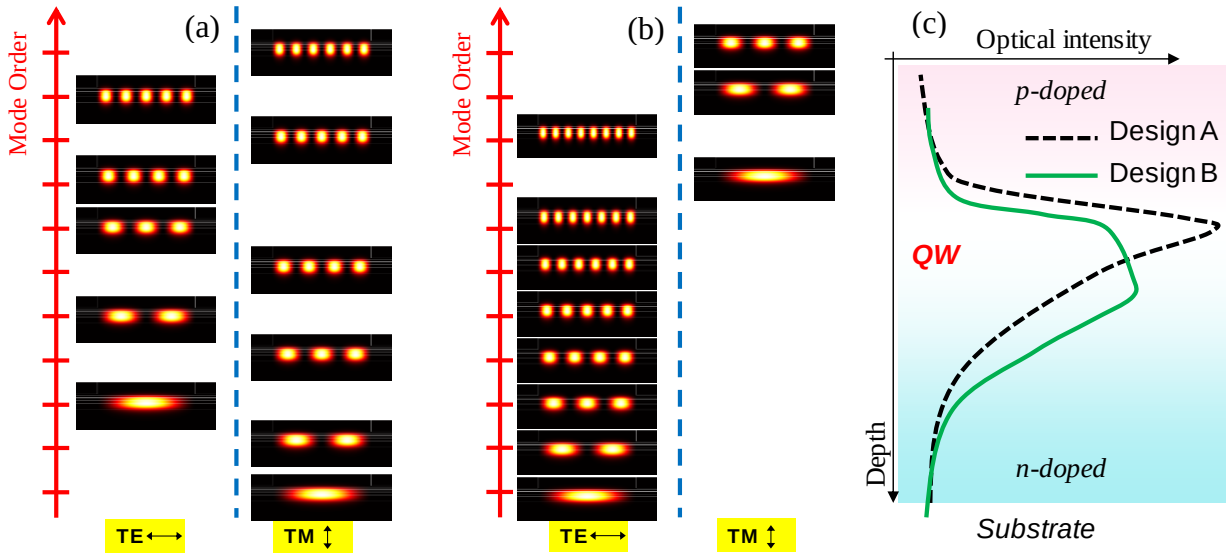

Figure 2. Simulation of the first 11 lateral modes in a cold cavity for epitaxial designs A (a) and B (b).
(c) Vertical waveguide design of an asymmetric epitaxial structure at 9xx nm wavelength for both designs.

Furthermore, with a careful engineering of the vertical waveguide layers to provide a large vertical spot size, we decreased the peak optical intensity in Design B, as seen in Figure 2(c), which, in turn, results in less pronounced nonlinearities and associated effects such as filamentation and spatial hole burning, thus subduing high-order lateral modes with a corresponding improvement of the far-field in the slow-axis (FFSA).

2.2 Single emitter performance & brightness

Both Design A and B wafers at 975 nm were processed into single emitters with a 95 µm lateral emission aperture. After cleaving, the chip facets were treated with our laser mirror passivation process [17] and coated with AR / HR coatings. Finally, the devices were assembled onto ceramic carriers and wirebonded to produce chip-on-carrier (CoC) parts for characterization. Note that our standard carriers and soldering process were used, without any optimization for strain relief or polarization enhancement.

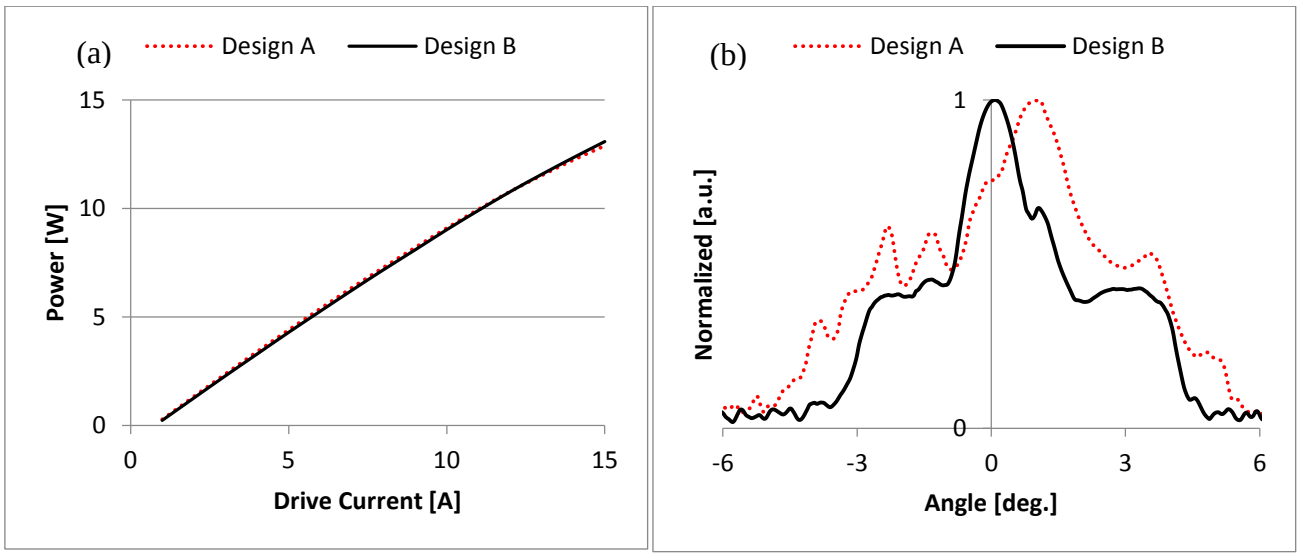

Figure 3. (a) Light-current characteristics of Design A and B emitters; (b) corresponding far-field slow-axis divergence.

At a heatsink temperature of 25°C under 15 A CW pumping, the lasers reach or exceed an average power of 13 W, with the light-current (*L-I*) characteristics shown in Figure 3(a). Design A devices are our baseline emitters rated for 12 A, 10 W reliable operation.

In contrast to the similarity in their *L-I* performance, the Design A and B emitters exhibit very different FFSA behavior as seen in Figure 3(b). Design A has an FFSA divergence of 10° at 14 W (at $1/e^2$ level). By contrast, the epitaxial structure optimization in Design B provides a narrowed FFSA with an 8° divergence, with a strong central peak suggesting the dominance of low-order lateral modes. This divergence corresponds to a slow-axis beam parameter product (BPP_{SA}) of 4.2 mm·mrad, or a brightness of 82 MW/sq.cm·sr.

3. POLARIZATION MEASUREMENTS

3.1 Polarization measurement setup

Two types of polarization measurement were performed. The first one, illustrated in Figure 4(a) and referred to as proximity DoP measurement, integrates over the entire laser emission at all angles to provide an integrated DoP_{int} metric, where both linear polarizer (LP) and power meter (PM) are placed immediately in front of the mounted laser, or CoC. The CoCs under test were operated in QCW mode (125 Hz on a 0.5% duty cycle), due to the damage threshold of the *Polarcor* linear polarizer, while sweeping the drive current up to 12A. At each current step, the TE and TM components of the emission were recorded by rotating the LP through 90°.

In the second type of measurement, which we call far-field angle-resolved, a directional DoP_{dir} is measured for a specific angular emission component. In this configuration, an uncollimated CoC is placed at a large distance from the LP on a rotation stage, with the PM and LP on a translation stage to ensure precise zeroing against the CoC emission axis. The entrance aperture captures a 0.5° angular slice from the laser emission, which could not be reduced further due to the low signal level on the PM. The setup enables rotation scanning in both the horizontal (slow axis) plane, Figure 4(b), and vertical (fast axis) plane, Figure 4(c). Here, the devices were operated in QCW mode at a constant current of 12 A.

Simultaneously with the polarization measurements, the far-field pattern was captured using a simple image processing technique, with the divergence angle computed as 97% content of the enclosed power.

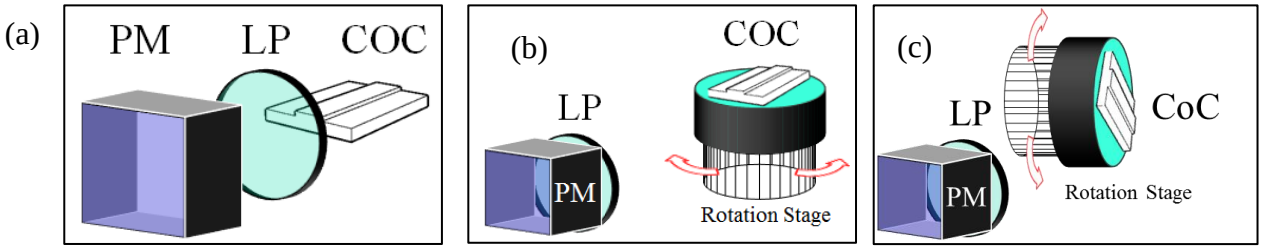

Figure 4.: (a) Proximity DoP_{int} setup, where the LP and PM are placed next to CoC; Slow-axis (b) and fast-axis (c) far-field angle-resolved DoP_{dir} setups.

3.2 Polarization behavior with drive current

On characterizing devices from Design A and B wafers using the proximity arrangement of Figure 4(a), we discovered very different behavior between the two designs. The measured DoP_{int} as a function of current are plotted in Figure 5, with the Design A devices only 94% TE-polarized at just above threshold and deteriorating with current towards 91%. By contrast, the Design B emitters both exhibited a higher DoP_{int} of 95% and maintained it at all operating currents.

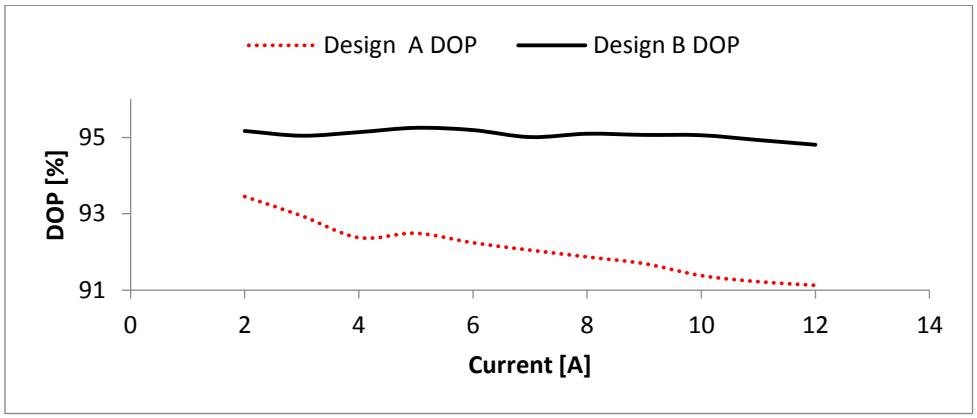

Figure 5. Proximity DoP_{int} measurement of Design A & B CoCs as a function of drive current.

To investigate the DoP_{int} deterioration in the Design A devices under high pumping, we correlated the observed DoP_{int} behavior with the FFSA divergence shown in Figure 6(a). The FFSA broadening, or blooming, in broad-area lasers with current is attributed to the excitation of high-order lateral modes with increasing far-field divergence [12], [18]. The correlation between the DoP_{int} and FFSA is even more pronounced in the graph of Figure 6(b), which plots their first derivatives to demonstrate that both undergo changes at the same currents.

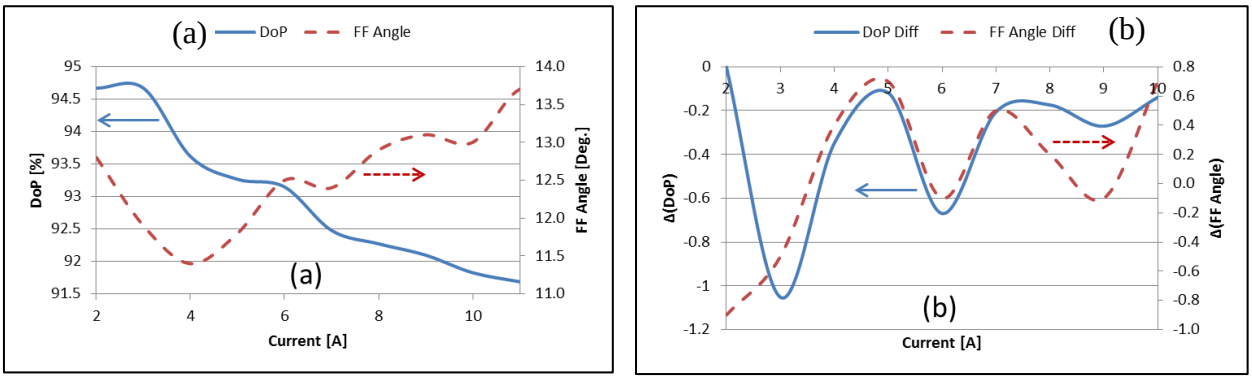

Figure 6. (a) Proximity TE DoP_{int} (solid) and FFSA divergence angle (dashed) for Design A devices as a function of current. (b) Differentials of the same data, showing high correlation.

Furthermore, by plotting the DoP_{int} and FFSA divergence in the Design A devices as a function of each other in Figure 7, one can see that these metrics exhibit substantially a linear interdependence, while no such correlation is discernable in Design B despite the limited FFSA blooming.

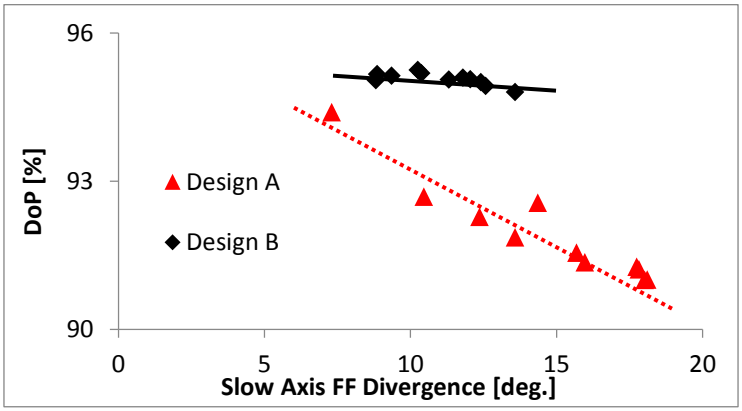

Figure 7. Proximity TE DoP_{int} as a function of FFSA divergence angle for Design A & B devices.

3.3 Angle-resolved polarization

In order to gain further insight into the intertwined DoP_{int} and FFSA behaviors, we performed angle-resolved DoP_{dir} measurements. First of all, we made sure that our results were invariant within the fast axis plane by characterizing the DoP_{dir} using the setup of Figure 4(c). Indeed, the fast-axis DoP remained substantially constant with angle as demonstrated in Figure 8(a) for both designs. Single transverse mode emission in the fast axis is consistent with a gonio-independent DoP_{dir} in that plane for a fixed slow-axis direction. The graph of Figure 8(a) also alleviates concerns about any signal level dependence in our DoP measurement, as off-axis intensities measured at large angles were two orders of magnitude below the on-axis intensity.

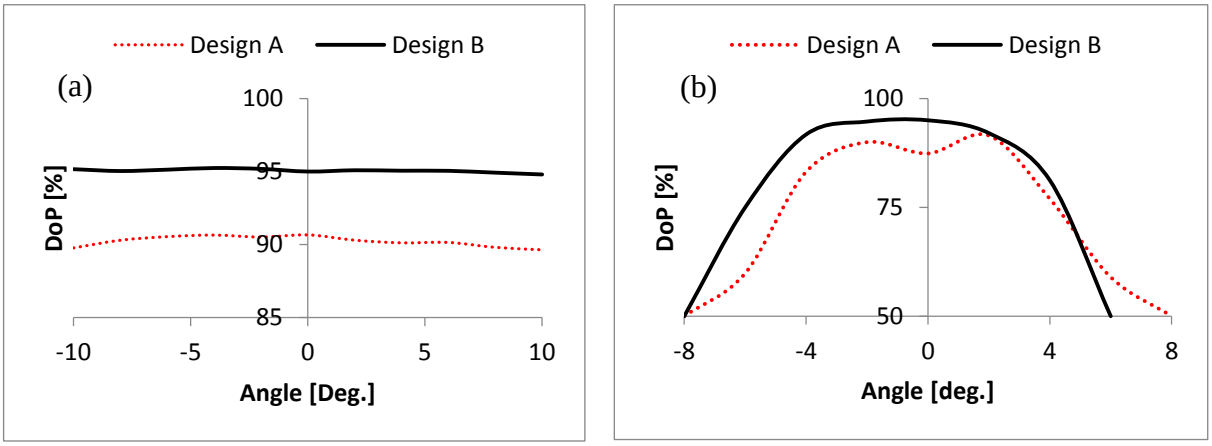

Figure 8. Angle-resolved DoP_{dir} in the fast (a) and slow (b) axes at 12 A current.

Conversely, the slow-axis measurements with the setup of Figure 4(b) produced the highly gonio-dependent DoP_{dir} patterns of Figure 8(b). It is important to emphasize that they do not to contain intensity information and should not be misconstrued as FFSA patterns. For example, the intensities used to compute the same DoP_{dir} of 50% at -8° for Designs A and B were very different, i.e., the intensity component at -8° in a Design B device was much weaker than in a Design A one due to the narrower FFSA of the former. While the graphs of Figure 8(b) both fall off to low DoP at large angles suggesting a growing TM content of high-order lateral modes, the small-angle behavior of Design A and B devices is markedly different. Not only do the Design B emitters provide a higher DoP_{dir} of 95%, they also maintain it over a broader FFSA angular range of about 6°.

4. SIMULATION & ANALYSIS

4.1 DoP simulation

The remarkable correlation between the DoP and FFSA observed in Figure 7 and Figure 8(b) provides interesting insights into the polarization properties of the modal content of the slow-axis emission. According to the waveguide models of Figure 2(a,b), high-order lateral modes come in alternating TE/TM polarization and are responsible for the DoP_{dir} degradation at large far-field angles as seen in Figure 8(b).

The difference at small angles, however, is that the Design B epitaxial waveguide favors low-order TE modes, which qualitatively explains the flat DoP_{dir} peak in Figure 8(b). By contrast, the lowest two modes in Design A are TM-polarized, which correlates with the central DoP_{dir} dip in that figure.

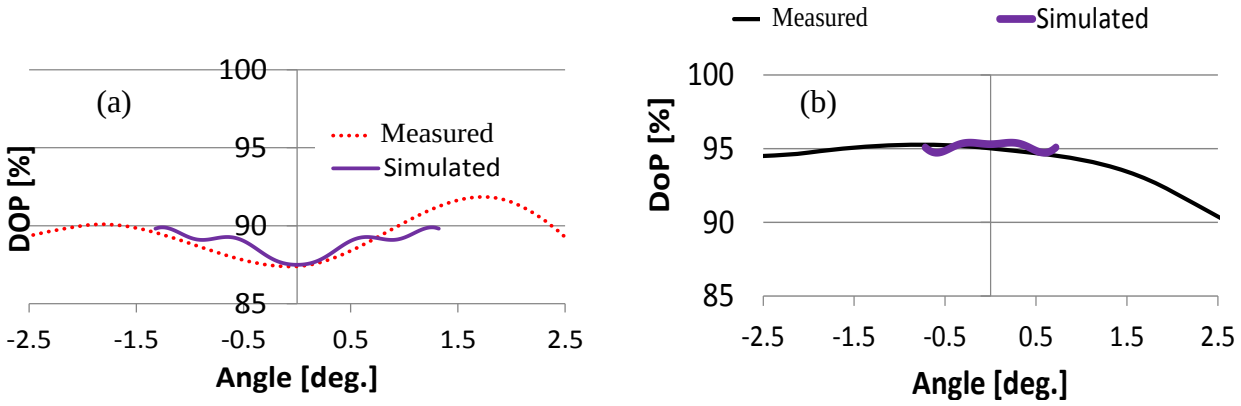

Figure 9. Measured and simulated DoP_{dir} as a function of FFSA angle for Design A(a) and B(b) emitters.

We also performed a basic simulation of the measured DoP_{dir} profiles using the mode structure of Figure 2(a,b) for the two epitaxial designs. At first, we built a superposition of the first 11 lateral modes and adjusted their relative intensities to reproduce the experimentally measured FFSA profiles, with the TM mode intensities chosen to be significantly lower than the TE ones. We then computed the angle-resolved DoP_{dir} according the weight of each mode, with the results plotted in Figure 9. With only 11 modes (and some of them having identical FFSA divergence for different TE and TM orders), we could only cover a small angular range of about ±1°, but nonetheless obtained a reasonably good agreement with the measured DoP_{dir}, especially the central trough in Figure 9(a) for Design A.

Arguably, the simulation is only very approximate and neglects other polarization selection mechanisms such as thermal waveguiding and strain fields around the etched trenches (on either side of the waveguide stripe) that cause parasitic TM-polarized emission [12]. Indeed, the enhancement of TM gain near the stripe edges directly contributes to high-order lateral modes that have intensity peaks in that region. However, the transverse-lateral waveguide design described in Sec.2 helps mitigate these effects through confinement and asymmetry engineering in favor of TE-polarized modes.

4.2 Polarization Brightness

The interplay between polarization and divergence described above has important ramifications for PBC schemes, especially in fiber-coupled multi-emitter modules, as in Figure 1. What really matters is the polarization-combinable power distribution, which we can formulate as a polarization-resolved FFSA:

$$FFSA_{TE}(\theta) = DoP_{dir\,TE}(\theta) \times FFSA(\theta)\,, \tag{2}$$

where $DoP_{dir\,TE}(\theta)$ represents the angular DoP profile of Figure 8(b). Therefore, the maximum polarization-combining efficiency is given by the convolution of the FFSA profile and angle-resolved DoP_{dir} normalized to the total energy:

$$DoP_{int\,TE} = \frac{\int DoP_{dir\,TE}\,(\theta) \times FFSA(\theta)\,d\theta}{\int FFSA(\theta)\,d\theta}, \tag{3}$$

which is equivalent to the proximity DoP_{int} measurement of Figure 4(a) as it integrates over all the emission angles.

In PBC context, we can now propose a definition for "polarization brightness", B_{TE}, which combines spatial brilliance and PBC efficiency:

$$B_{TE} = DoP_{dir\,TE} \times \frac{Power}{\pi^2 BPP_{FA} BPP_{SA}} \tag{4}$$

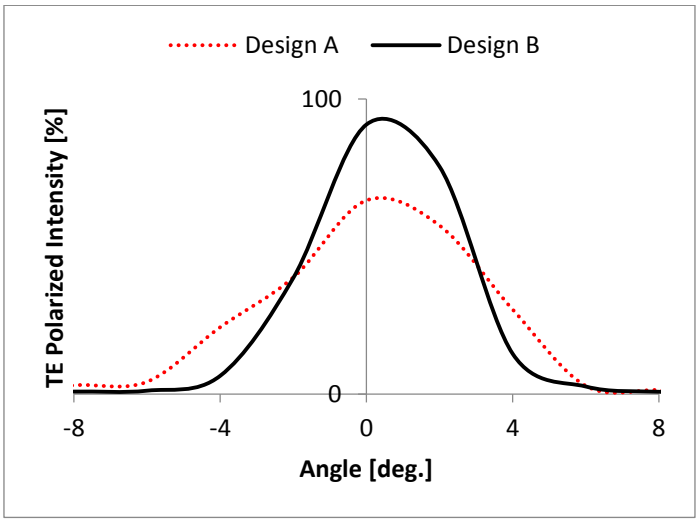

Figure 10. TE polarized FFSA intensity of Design A and B devices.

The application of the above definitions to emitters from Designs A and B is illustrated in Figure 10, which is obtained by Eq.(2). In juxtaposition with the FFSA-only profiles of Figure 3(b), the polarization-resolved distributions of Figure 10 highlight the double benefit of Design B over A: (1) the narrower divergence; and (2) higher TE DoP_{int} within that divergence. The area integral of Eq.(3) under the Design B curve is also larger resulting in higher η_{TE} and higher polarization brightness B_{TE}, which is further amplified by the low BPP_{SA} of the Design B devices in Eq.(4).

Recalling the brightness of 82 MW/sq.cm·sr for Design B emitters in Sec. 2.2 with a measured η_{TE} of 95%, we obtain a B_{TE} of 78 MW/sq.cm·sr. This number represents the maximum brightness of a polarization-combined multi-emitter system based on Design B devices.

5. CONCLUSIONS

We have presented the development of high "polarization brightness" single emitters optimized for both high PBC efficiency and high fiber coupling efficiency. The improvement is achieved by careful transverse-lateral waveguide engineering, first to increase the spatial brightness through lower filamentation and associated nonlinearities, and then to enhance guiding for TE-polarized lateral modes. The resulting devices exhibit both lower BPP_{SA} and higher DoP than emitters fabricated from our baseline epitaxial design.

With further optimization of the device design such as metallization thickness, and a better-matched, low-stress packaging platform and soldering process, we expect emitters based on our latest epitaxy to reach DoP benchmarks in excess of 95%.

We further demonstrated the interdependence between slow-axis divergence and polarization, which prompted us to introduce polarization brightness as a metric for PBC applications.

ACKNOWLEDGEMENTS

The authors would like to thank S. Geva and D. Weiss for their technical assistance with the fabrication, assembly and characterization of the laser devices presented here.

REFERENCES

[1] L. Vaissie, T. Steele, and P. Rudy. "High-power diode lasers advance pumping applications." Laser Focus World (June 2008).

[2] B.O. Faircloth, "High-brightness high-power fiber coupled diode laser system for material processing and laser pumping", *Proc. SPIE* 4973, *High-Power Diode Laser Technology and Applications*, 34 (June 18, 2003); doi:10.1117/12.478365.

[3] E. Zucker, D. Zou, L. Zavala, H. Yu, P. Yalamanchili, et al., "Advancements in laser diode chip and packaging technologies for application in kW-class fiber laser pumping", *Proc. SPIE* 8965, *High-Power Diode Laser Technology and Applications* XII, 896507 (March 7, 2014); doi:10.1117/12.2038268.

[4] N. P. Ostrom, M. Gall, and B. O. Faircloth, "Development of high power high brightness fiber coupled diode laser systems", *Proc. SPIE* 6104, *High-Power Diode Laser Technology and Applications* IV, 61040N (February 15, 2006); doi:10.1117/12.660635.

[5] B. Köhler, S. Ahlert, A. Bayer, H. Kissel, H. Müntz, et al., "Scalable high-power and high-brightness fiber coupled diode laser devices", *Proc. SPIE* 8241, *High-Power Diode Laser Technology and Applications X*, 824108 (February 9, 2012); doi:10.1117/12.909189.

[6] T.S. Fan, A. Sanchez, V. Daneu, R.L. Aggarwal, S.C. Buchter, A. Goyal, and C.C. Cook. "Laser beam combining for power and brightness scaling," In *IEEE Aerospace Conference Proceedings*, vol. 3, pp. 49-54., 2000.

[7] T.S. Fan, "Laser beam combining for high-power, high-radiance sources," *IEEE J. Sel. Topics in Q. Elec.*, 11 No. 3, 2005, pp. 567-577.

[8] A. Al-Qasimi, O. Korotkova, D. James, and E. Wolf, "Definitions of the degree of polarization of a light beam," *Optics Letters* 32, No. 9, 2007, pp.1015-1016.

[9] V.V. Bliznyuk, et al. "Degradation and spectral–spatial characteristics of the radiation of high-power laser diodes," *Bulletin of the Russian Academy of Sciences: Physics* 79, No.12, 2015, pp. 1458-1463.

[10] M. Weyers *et al.*, "Epitaxy of high-power diode laser structures, strained quantum wells," in *High-Power diode lasers*, edited by R. Diehl (Springer Verlag, Berlin, 2000), Chap. 5, p. 107.

[11] M. G. Daly, D. M. Bruce, P. E. Jessop, D.T. Cassidy, and D. Yevick, "Metallization stress in weakly guiding InP/InGaAsP waveguides," *Semiconductor Science and Technology* 9, No. 7, 1994, p.1387.

[12] M. Winterfeldt, P. Crump, H. Wenzel, G. Erbert, and G. Tränkle. "Experimental investigation of factors limiting slow axis beam quality in 9xx nm high power broad area diode lasers." *J. App. Phys.* 116, No. 6, 2014, 063103.

[13] D. Yanson, N. Rappaport, M. Shamay, S. Cohen, Yuri Berk, et al. "High-power single emitters for fiber laser pumping across 8xx nm – 9xx nm wavelength bands", Proc. SPIE 8241, High-Power Diode Laser Technology and Applications X, 82410A (February 9, 2012); doi:10.1117/12.909016.

[14] D. Yanson, N. Rappaport, M. Shamay, S. Cohen, Yuri Berk, et al. "Brightness-enhanced high-efficiency single emitters for fiber laser pumping", Proc. SPIE 8605, High-Power Diode Laser Technology and Applications XI, 860505 (February 26, 2013); doi:10.1117/12.2003838.

[15] D. Labukhin and X. Li, "Polarization insensitive asymmetric ridge waveguide design for semiconductor optical amplifiers and super luminescent light-emitting diodes." *IEEE J. Quan. Elec.* 42, No. 11, 2006, pp. 1137-1143.

[16] R. J. Lang, A. G. Larsson and J. G. Cody, "Lateral modes of broad area semiconductor lasers: theory and experiment," in *IEEE J. of Q. Elec.*, vol. 27, no. 3, pp. 312-320, Mar 1991. doi: 10.1109/3.81329.

[17] D. Yanson, M. Levy, M. Shamay, R. Tesler, N. Rappaport, Y. Don, Y. Karni, I. Schnitzer, N. Sicron, and S. Shusterman, "Facet engineering of high power single emitters," *Proc. SPIE* 7918, *High-Power Diode Laser Technology and Applications* IX, 79180Z (21 February 2011); doi: 10.1117/12.876261.

[18] J. Piprek, "Self-consistent far-field blooming analysis for high-power Fabry-Perot laser diodes", *Proc. SPIE* 8619, *Physics and Simulation of Optoelectronic Devices* XXI, 861910 (March 14, 2013); doi:10.1117/12.2004665.